Kuwait J.Sci., Vol.48, No.(3),July.2021,pp(1-10)

# Hydrothermally growth of $TiO_2$ Nanorods, characterization and annealing temperature effect

[1]Nada Falih M.,[2]Saleem Azara Hussain,[3]Shawki Khalaf Muhammad
[1]Adel H. Omran Alkhayatt*
*[1]Faculty of Science, University of Kuf, Iraq*
*[2]College of Education, University of Al Qadisiyah, Iraq*
*[3]Faculty of Education for Girls, University of Kufa, Iraq*
**Corresponding author: adilh.alkhayat@uokufa.edu.iq*

## Abstracts

Titanium dioxide $TiO_2$ nanorods were successfully grown on conductive glass FTO substrate using the hydrothermal method at a temperature of 160 oC. Surface topography, structure, and optical characteristics were studied according to the influence of annealing temperature (450, 550, and 650) oC. The surface topography results reveal that the $TiO_2$ had nanorods structure with a tetragonal shape, and the rod diameter increases from 84.2 nm to 116.6 nm with increasing the annealing temperature. The crystal structure of the grown $TiO_2$ NRs exhibits a high crystallinity of polycrystalline nature with anatase and rutile phases. The preferential orientation was along (204) plane for anatase tetragonal structure. AFM image shows an intense edge, uniform surface morphology, and increased grain diameter with annealing temperature. The optical properties of $TiO_2$ NRs were investigated, and the absorption edge shows a blue shifting as the annealing temperature increases when considering the crystallinity and morphology changes. The energy band gap was found to be lower than 3 eV, which can be attributed to the presence of anatase and rutile phases with an increment range from 2.72 to 2.86 nm alongside the increase in the annealing temperature. The results indicate that the adopted hydrothermal method and the synthesized $TiO_2$ NRs were suitable for photovoltaic and photocatalytic applications.

**Keywords:** Anatase and rutile phases; annealing effect $TiO_2$ nanorods; hydrothermal method; surface morphology.

## 1.Introduction

Titania ($TiO_2$) is one of the well-known titanium compounds that is often used in various applications. These include anti-corrosion, self-cleaning coatings, photovoltaics, photocatalysis, and ordinary and dye synthesized solar cells (Keerthana et al., 2018). There are three different phases for a crystalline form of $TiO_2$: rutile, anatase phases of (tetragonal structure) and brookite of (orthorhombic structure) (Khataee and Mansoori, 2011). Both anatase and rutile are belonging to different phase groups despite the they have a tetragonal crystal structure. Rutile $TiO_2$ has a higher (refractive index, electric resistance, dielectric constant, and chemical stability) than that of the anatase phase (Tsevis et al., 1998). At low temperatures and acidic medium, brookite is often observed (Komaraiah et al., 2016). Bulk $TiO_2$ is known to be a much useful, environmentally friendly, non-toxic, corrosion-resistant material, sun-blockers, frequently used in paint and white pigments for its white color. It is an n-type semiconductor material with an energy band gap of 3.02 eV for rutile, 3.23 eV for anatase, and 3.13 eV for brookite (Tang et al., 1995; Suslick, 1998; Oja et al., 2004; Bedikyan et al., 2013; Martínez et al., 2018; Byranvand et al., 2013; Seifried et al., 2000; Palmisano et al., 1988). $TiO_2$ nanostructure can be grown using many various methods

such as chloride process (Suslick, 1998), spray pyrolysis (Oja et al., 2004), sputtering (Bedikyan et al., 2013), Sol-gel method (Martínez et al., 2018), chemical vapor deposition (Byranvand et al., 2013), Physical Vapor Deposition (PVD) (Seifried et al., 2000) and hydrothermal method (Palmisano et al., 1988). Hydrothermal synthesis is the technique used to fabricate materials at low temperatures with high vapor pressure. Because the reaction is conducted in conditions with a closed system, this method is considered the most environmentally friendly and saves energy (Zheng, 2016; Idris 2015). Teflon-lined stainless steel autoclave is usually used in hydrothermal synthesis under controlled temperature in aqueous solutions (Bregadiolli et al., 2017). The materials that are synthesized by the hydrothermal method have many specifications. This includes a high purity, good homogeneity, and crystalline safety with narrow grain size distribution (Wirunmongkol et al., 2013). The latter method is a successful way to prepare nanoscale of ZnO, $TiO_2$, and other brilliant materials (Reddy et al., 2015).

In the present work, vertically aligned $TiO_2$ Nanorods were successfully synthesized from TiCl4 using a facile way hydrothermal method at low reaction temperature (160 oC) and time (7 h). The effect of high annealing temperatures (450-650) oC on the structural, surface morphology, and the optical band gap was investigated.

## 2. Experimental details

### 2.1. Materials and methods

Hydrochloric acid (HCl) (SDFCL, 35.4%) and Titanium tetrachloride (TiCl4) (BDH, wt% 99.0) were used. The fluorine-doped tin oxide (FTO) conductive glass was used as a substrate for $TiO_2$ NRs thin film deposition. The distilled water was produced in the laboratory. A 40 mL of HCl (6 M) and 0.3 ml of TiCl4 were mixed using a magnetic stirrer for 15 min. Then, three slides of FTO glass were vertically inserted into the Teflon-lined, which were previously ultrasonically cleaned in the sequence of propanol and acetone for 10 min individually. A 30 ml of the prepared solution was added to the Teflon-lined stainless steel autoclave (40 ml), heated in an oven up to 160 °C for 7 h, and then cooled to room temperature. The substrates were taken out of the autoclave, dried, and annealed at 450, 550, and 650 °C for 1 h. Finally, a white layer of $TiO_2$ NRs was obtained on the surface of the FTO substrate.

### 2.2. Characterizations

Structural characterizations of $TiO_2$ nanostructure films were performed using X-ray diffraction (X-Ray Diffractometer, DX-2700) with Cu kα. The scanning angle varied in the range of (10-70)° at a room temperature with a wavelength of 1.5406 Å. The surface morphologies were characterized using field mission scanning electron microscope FE-SEM (FEI FESEM Nova 450, FEI-Netherlands-Holland). The topography of $TiO_2$ nanostructure was studied using atomic force microscopy (CPSM model AA3000 supply by Angstrom Company). The optical characterization was studied from the outcome of the absorbance and transmittance in the UV-Vis region (300-900)nm using a double beam Mega 2100-Sinco UV-Vis spectrophotometer.

## 3. Results and discussion

The $TiO_2$ nanostructures micrographs obtained from the field emission scanning electron microscopy (FESEM) on FTO substrate annealed at different temperatures are illustrated in Figure1 (a, b and c). The micrographs reveal that the $TiO_2$ has a nanorods structure with a tetragonal shape; their diameters were increased from 84.2 nm to 100 and then to 116.6 nm with the increase of annealing temperature. It can be noticed that there is no difference in the surface morphology, which can be observed among the samples. The latter indicates that

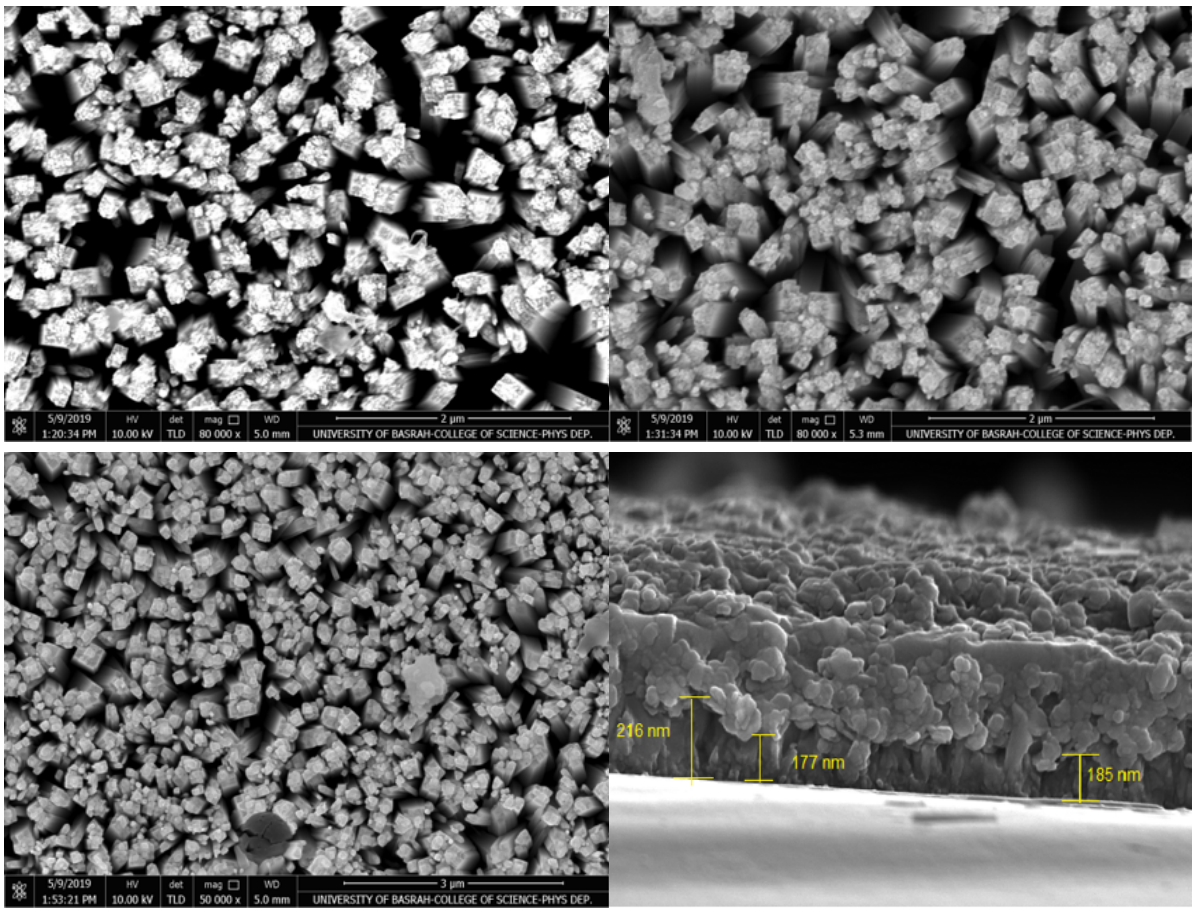


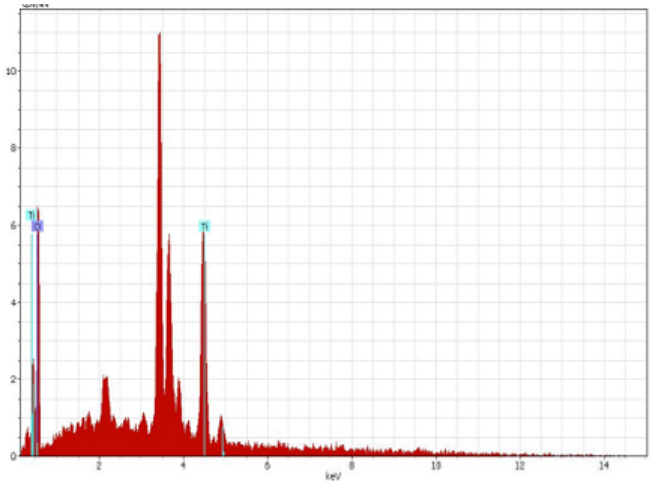


**Fig. 1.** FESEM micrographs of $TiO_2$ NRs at the annealing temperature.
(a) 450 oC, (b) 550 oC, (c) 650 oC, (d) cross section and (e) EDX spectrum for $TiO_2$ NRs at Ta

X-ray diffraction measurements and analysis were utilized to determine the structural characterizations and phase formation. Figure 2. illustrates the XRD pattern of $TiO_2$ nanostructures deposited on FTO substrate, which was annealed at different temperatures. The strong and distinctive $TiO_2$ peaks were found for the samples that annealed at (450, 550, and 650) oC in the diffraction angles of 26.94°, 26.91° and 27.0° 36.23°, 36.42°, 36.30°, 38.07°, 38.22°, 38.12°, 51.67°, 51.84°, 51.60°, 62.63°, 62.72°, 62.58°, and 66.36°, 66.39°, 66.30° respectively. These diffraction peaks were assigned to the mixed phases of anatase, rutile $TiO_2$ and FTO structure,

which corresponding to R(110), R(101), A(004), FTO(211), A(204), and R(221) crystal planes and well matching with JCPDS cards A(21-1272), R(21-1276) and FTO(41-1445) as shown in the figure. The preferential orientation was clearly observed along the (204) plane for the anatase phase and tetragonal structure. The intensity of diffraction peaks was slightly increased with annealing temperature, which indicates that the crystallinity of nanostructure $TiO_2$ was enhanced. These results agreed with the literature (Li et al., 2019; Huang et al., 2019; Liao et al., 2015). Table 1. shows the lattice constants a and c which were calculated for the anatase tetragonal structure of $TiO_2$ nanostructure at different annealing temperature using the equation (Alkhayatt and Hussian, 2015):

$$\frac{1}{d^2}=\frac{h^2+k^2}{a^2}+\frac{l^2}{c^2} \qquad (1)$$

Where d is the interplanar spacing, and (hkl) Miller indices, the lattice constants a and c values (as shown in Table.1) are well-matched with (JCPDS anatas-21-1272) values, a is (3.7852 Å), and c is (9.5139Å). Moreover, the interplanar spacing dhkl values were calculated using Bragg›s law and matching JCPDS values.

The average crystallite size D of nanostructure $TiO_2$ films were calculated using the Debye-Scherrer equation as shown in (Table 1) (Alkhayatta et al., 2018):

$$D=\frac{k\lambda}{\beta cos\theta} \qquad (2)$$

where k is the shape factor (equal to 0.94), λ is the X-ray wavelength (1.5406 Å), and β is defined as the full width at half maximum (FWHM), respectively, whereas Θ is the diffraction angle. It was found that the average crystallite size values in the range of 21.48 to 23.63 nm for the anatase phase. This observation indicates that the crystallite size of nanostructure $TiO_2$ decreased then increased slightly with the increase of annealing temperature. The slight variation of the crystallite size could be responsible for the intensity variation in the diffraction peak. The result was consistent with the published literature (Manikandan et al., 2015). The dislocation density (δ) and microstrain (ε) of the prepared samples was evaluated using Williamson and Smallman formula (Li et al., 2019; Jaafer et al., 2019):

$$\delta=\frac{1}{D^2} \qquad (3)$$

and

$$\varepsilon=\frac{\beta\cos\theta}{4} \qquad (4)$$

The dislocation density is the number of dislocation lines per unit area, and it shows the opposite behavior of the crystallite size with the increase of annealing temperatures (see Table 1). The number of dislocations increases with increasing the grain boundaries which contains the dislocations and the structure defects, while dislocations defects decreased with the reduction of the grain boundaries due to the variation of the crystallite size (Li et al., 2019; Huang et al., 2019; Zgaira et al., 2019). The lattice microstrains increase gradually decrease with the increase of the annealing temperature from 450 to 650°C, as illustrated in Table (1). This indicates that the strain relaxation occurs during the heat treatment and following the literature (Rožić et al., 2019; Malevu et al., 2019). The anatase to rutile phase transformation plays an important role in the physical properties of $TiO_2$, which is related to the variation in the structural defects, which lead to variation in the optical and electrical properties of the prepared samples (Moamen et al., 2018). The rutile-to-anatase ratio of the synthesized $TiO_2$ samples at different annealing temperatures was calculated using XRD results. It was found that the rutile/anatase (IR/IA) ratio of $TiO_2$ annealed at 450°C is 0.107, i.e., the anatase phase is a major phase. This ratio increases with the increase of annealing temperature to 550°C, which confirms that anatase-to-rutile transformation increases. Whereas the rutile/anatase ratio was decreased to the lower value of 0.09 at annealing temperature

650°C, which means the anatase-to-rutile transformation reduced and may reduce the structural defects within the electronic band structure (Moamen et al., 2018).

To investigate the surface topography of the synthesized $TiO_2$ nanorods, AFM analysis was performed. The height profile of the $TiO_2$ NRs is shown in Figure 3. AFM

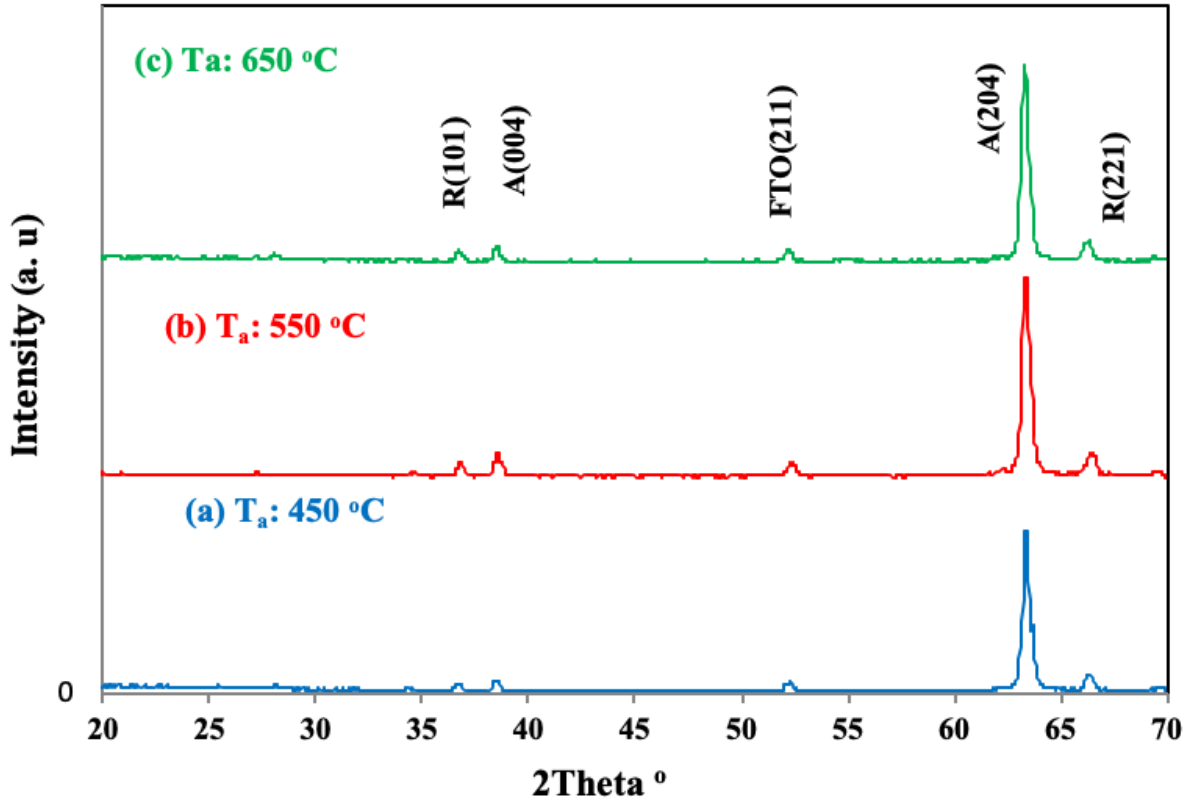


**Fig. 2.** XRD patterns of $TiO_2$ NRs deposited on FTO for different annealing temperature (a) 450°C, (b) 550°C, (c) 650°C.

**Table 1.** The XRD results of $TiO_2$ NRs anatase phase for (204) plan.

| $TiO_2$ $T_a$ °C | 2theta | $d_{hkl}$ (XRD) | $d_{hkl}$ (JPCDS) | $a_{hkl}$ | $c_{hkl}$ | (FWHM) | D (nm) | $\delta*10^{14}$ (line/m$^2$) | $\varepsilon*10^{-4}$ |
|---|---|---|---|---|---|---|---|---|---|
| 450 | 62.64 | 1.4818 | 1.4808 | 3.8087 | 9.4268 | 0.361 | 23.11 | 18.72 | 15.66 |
| 550 | 62.72 | 1.4799 | 1.4808 | 3.8094 | 9.4124 | 0.387 | 21.48 | 21.66 | 16.85 |
| 650 | 62.58 | 1.4831 | 1.4808 | 3.8172 | 9.4348 | 0.354 | 23.63 | 17.90 | 15.32 |

image shows the intense edge, uniform surface morphology, and a spherical feature observed on the surface. Table 2. illustrates the average roughness, root means square, and the grains average diameter for each sample. Surface Roughness and RMS Roughness were increased and then decreased by increasing annealing temperature from 450 to 550°Cand then to 650°C, while the grain diameter was decreased and then increased.

These results indicate that the surface morphology was strongly dependent upon the annealing temperature, while the dramatic morphology change may be due to the crystallinity of the prepared $TiO_2$ NRs with the increase of annealing temperature. The results are well matched with XRD results and agreed with the findings reported by (Muaz et al., 2015; Bakri et al. 2017).

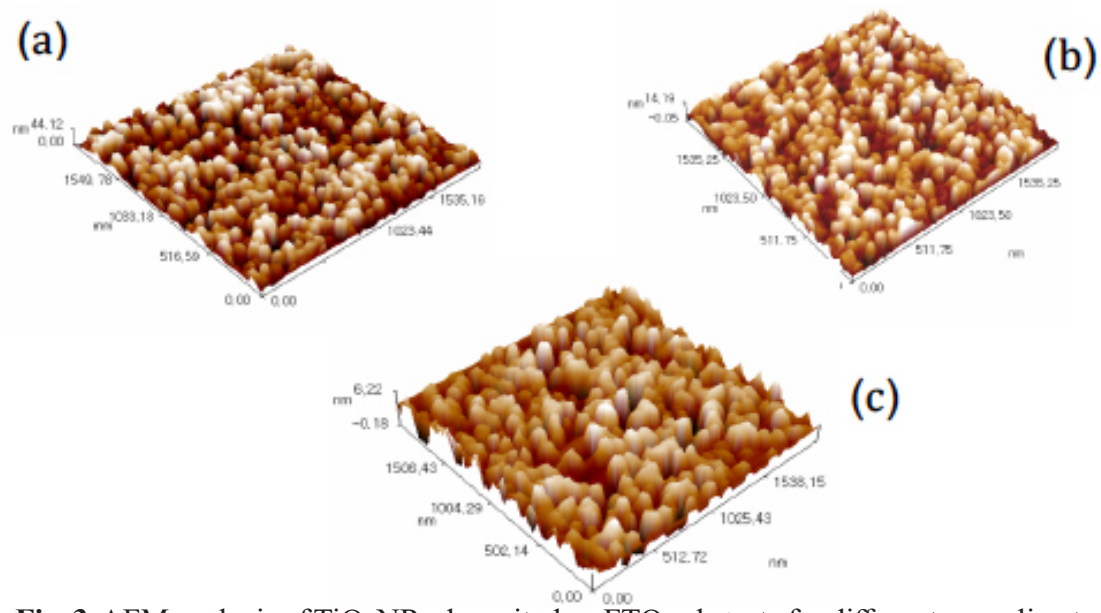


**Fig. 3.** AFM analysis of $TiO_2$ NRs deposited on FTO substrate for different annealing temperature (a) 450 oC, (b) 550 oC, (c) 650 oC.

**Table 2.** AFM analysis results of $TiO_2$ NRs annealed at 450, 550, and 650 oC temperatures.

| $TiO_2$ Ta °C | Roughness Avg. (nm) | Root mean square (nm) | Avg. Diameter (nm) |
|---|---|---|---|
| 450 | 2.93 | 3.47 | 79.33 |
| 550 | 11 | 12.8 | 65.15 |
| 650 | 1.25 | 1.51 | 94.68 |

The UV-Vis transmittance spectra were investigated to study the influence of annealing temperature on the absorption edge of $TiO_2$ NRs. Figure (4 a and b) shows the optical transmittance and the optical absorbance spectra corresponding to Tauc relation (Alkhayatt et al., 2019; Kokaj et al., 2018; Sumaryada et al., 2019):

$$(\alpha h\upsilon)^2 = A(h\upsilon - Eg) \qquad (5)$$

Where A is constant, α is the absorption coefficient; Eg is the optical energy gap, ν is the frequency of the incident photon, h is the Planck constant. The transmittance was very low in the UV region and at the beginning of the Vis region because of the absorption edge of $TiO_2$, then it rapidly increases with the increase of visible wavelengths and reaches its higher values of about 75% at the NIR region. The transmittance was varied with random sequence, with the increase of annealing temperature as shown in figure (4a), which can be related to the variation of the crystallite size and grain diameter, which led to varying the dislocation and the scattering centers due to the crystal defects at the grain boundaries (Keskenler et al., 2012; Alkhayatt and Hussian 2017) [34, 35]. The influence of increment of annealing temperature on the optical energy gap of $TiO_2$ NRs was determined by using equation (5). From Figure 4 a, in general, it can be seen that the absorption edge was red-shifted towards long wavelengths and low energies by the increase of annealing temperature, which can be referred to as the enhancement of $TiO_2$ NRs crystallinity (Allam and El-Sayed, 2010). Therefore, the optical energy

gap value for the direct transition was decreased from 2.81 eV to 2.77 eV and then increment to 2.835 eV with the increment of annealing temperature from 450 to 550 oC and 650 oC, respectively. This variation in the energy gap of the annealed $TiO_2$ NRs can be attributed to the structure and morphology of the NRs where the average crystallite size and the average grain diameter were decreased at annealing temperature 550 oC, which led to increasing of crystal defects and, in turn, the defects levels introduced into the bandgap and reduced the forbidden gap. On the other hand, the crystallite size and the grain diameters were increased at an annealing temperature of 650 oC, so the crystal defects were reduced. The defect levels were removed from the bandgap and widening the energy gap. These results were consistent with the literature (Daneshvar et al., 2019; Alkhayatt et al., 2018) [20, 23]. The energy gap values were lower than 3 eV; the narrowing of the band gap can be attributed to the existence of structural defects in the synthesized $TiO_2$ nanorods. Where the decrease in the crystallite size and particle size leads to the increase in the ratio of surface to bulk defects and, in turn, increased the conduction and valence bands tailing, resulting in a narrower band gap (El-Sayed et al., 2017; Soliman et al., 2018).

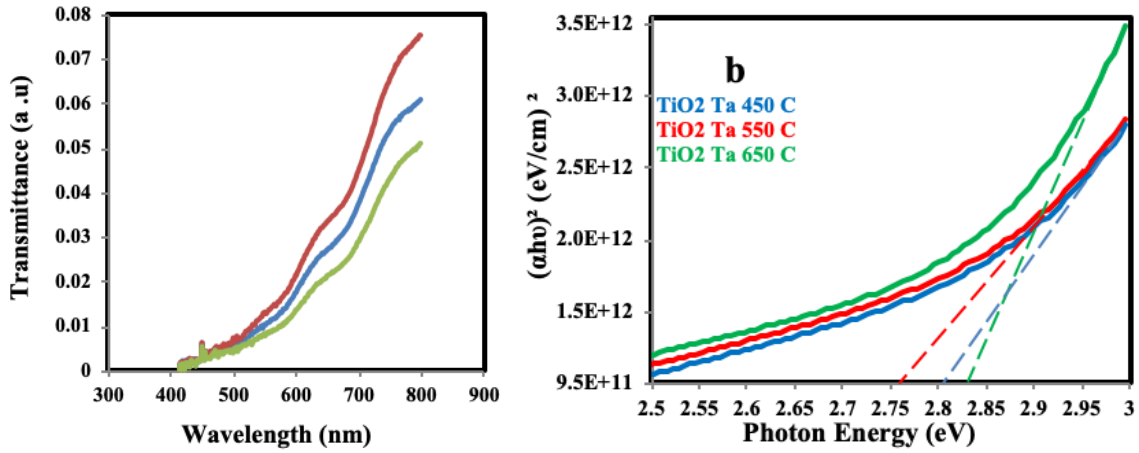


**Fig. 4.** (a) UV–Vis Transmittance spectra and (b) optical band gap of $TiO_2$ NRs annealed at 450 oC, 550, and 650 oC temperatures.

## 4. Conclusion

$TiO_2$ nanorods were successfully synthesized on FTO conductive glass substrate by the hydrothermal method. The deposition parameters and conditions were as follows: 6 M concentration of HCl, 160 oC and 7 h reaction temperature and time, 0.3 ml of TiCl4 solution content, 450 C°, 550 °C, and 650 °C annealing temperatures, for 1 h were selected as the optimal conditions. Surface topography results reveal that the nanorods were tetragonal in shape, quadrate face diameter of the nanorods was 84.2 nm, 100 to 116.6 nm as annealing temperature increased. $TiO_2$ nanorods were arranged in the xz plane, i.e., they prefer to grow in the plane (204) of the tetragonal anatase $TiO_2$ crystal. XRD results show the successfully fabricated $TiO_2$ nanorods with the desired size and preferential anatase phase using titanium tetrachloride as a starting material. The optical transmittance was increased, and the fundamental absorption edge was blue-shifted with the increase of annealing temperature. The obtained results indicate that $TiO_2$ NRs material is very suitable for photovoltaics and photocatalysis applications.

## ACKNOWLEDGEMENTS

The authors are very grateful for to assistance that offered by the advanced thin films lab. And physics department in the Faulty of science University of Kufa Iraq, Prof. Dr. Mazin Auny Mahdi Department of Physics in the College of Science, University of Basrah. Also, we are very grateful to Prof. Dr. Hussien Abid Ali Bakir Mraity, Faulty of science University of Kufa, for his assistance in the English language editing of the manuscript.

## References

**Abdelhafiz, A.; Ganzoury, M.; Amer, A.; Faiad, A.; Khalifa, A. et al. (2018).** Defect Engineering in 1D Ti-W Oxide Nanotube Arrays and Their Correlated Photoelectrochemical Performance Physical Chemistry Chemical Physics **20** (15): 10258-10265.

**Alkhayatt, A. and Hussian, S. (2015).** Fluorine highlydopednanocrystalline$SnO_2$ thin films prepared by SPDn technique Materials Letters, **155**: 109-113.

**Alkhayatt, A. and Hussian, S. (2017).** Fluorine dopant concentration effect on the structural and optical properties of spray deposited nanocrystalline ZnO thin films Surfaces and Interfaces **8**: 176-181.

**Alkhayatt, A.; Hussain, S. and Mahdi, E. (2018).** An investigation into the impact of Ti doping on the structural, optical, and sensing properties of spray deposited nanocrystalline $ZrO_2$ thin films. Optik, **159**: 305-314.

**Alkhayatt, A.; Habieb, A.; Al-Noaman, A., and Hameed, A. (2019).** Structure, surface morphology, and optical properties of CuxZn1-xS/Au NPs layer for photodetector application The 1st International Scientific Conference on Pure Science IOP Conf. Series: Journal of Physics: Conf. Series 1234: 012012.

**Allam, N. K. and El-Sayed, M. (2010).** Photoelectrochemical Water Oxidation Characteristics of Anodically Fabricated $TiO_2$ Nanotube Arrays: Structural and Optical Properties. J. Phys. Chem., **114**: 12024–12029.

**Bakri, A.; Sahdan, M.; Adriyanto, F.; Raship, N.; Said, N. et al. (2017).** Effect of annealing temperature of titanium dioxide thin films on structural and electrical properties. International Conference on Engineering, Science and Nanotechnology, AIP Conf. Proc. 1788: 030030.

**Bedikyan, L.; Zakhariev, S. and Zakharieva, M. (2013).** Titanium Dioxide Thin Films: Preparation and Optical properties. (2013). J. Chem. Technol. Metall. **48**: 555-558.

**Bregadiolli, B.; Fernandes, S. and Graeff, C. (2017).** Easy and Fast Preparation of $TiO_2$ - based Nanostructures Using Microwave Assisted Hydrothermal Synthesis. Materials Research, **20**(4): 912-919.

**Byranvand, M.; Kharat, A.; Fatholahi, L., and Beiranvand Z. (2013).** A Review on Synthesis of Nano-$TiO_2$ via Different Methods J. nanostructures **3**: 1-9.

**Daneshvare, S.; Saed, A. and Sadrnezhaad, S. (2019).** Hierarchical rutile/anatase $TiO_2$ nanorod/nanoflower thin film: Synthesis and characterizations. Materials Science in Semiconductor Processing, **93**: 252-259.

**Dussan, A.; Bohórquez, A. and Quiroz, H. (2017).** Effect of annealing process in $TiO_2$ thin films: Structural, morphological, and optical properties. Applied Surface Science **424**: 111-114.

**El-Sayed, A.; Atef, N.; Hegazy, A.; Mahmoud, K.; Abdel Hameed, R. et al. (2017).** Defect states determined the performance of dopant-free anatase nanocrystals in solar fuel cells. Solar Energy **144**: 445–452.

**Etacheri, V.; Seery, M.K.; Hinder, S.J.; and Pillai, S.C., (2011).** Oxygen-rich Titania: a dopant-free, high temperature stable, and visible-light active anatase photocatalyst. Adv. Funct. Mater. **21**: 3744–3752.

**Huang, H.; Hou, X.; Xiao, J.; Zhao, L.; Huang, Q. et al. (2019).** Effect of annealing atmosphere on the performance of $TiO_2$ nanorod arrays in photoelectrochemical water splitting Catalysis Today, **330**: 189-194.

**Idris, W., Characterization of Nanostructure ZnO Synthesized Through hydrothermal Method (2015).** MS.c. Thesis, Universiti Tun Hussein Onn, Malaysia.

**Jaafer M, M.; Alkhayatt, A. and Saleh, S. (2019).** Structural, Surface Topography and Optical Characterization of Nanocrystalline MgxZn1-xO Thin Films Grown by Modified Chemical Bath Deposition (SILAR) Method. J. Phys.: Conf. The 1st International Scientific Conference on Pure Science IOP Conf. Series: Journal of Physics: Conf. Series, 1234: 012001.

**Keerthana, B.; Solaiyammal, T.; Muniyappan, S.; and P Murugakoothan, P. (2018).** Hydrothermal synthesis and characterization of $TiO_2$ nanostructures prepared using different solvents. Mater. Lett. **220**: 20-23.

**Keskenler, E.; Turgut, G.; Aydin, S. and Dogan, S. (2012).** Effects of fluorine incorporation on the microstructure and optical properties of ZnO thin films synthesized by Sol-gel technique. Sci. Res. Essays **7**(44): 3816-3822.

**Khataee, A., and Mansoori G., (2011)** Nanostructured Titanium Dioxide Materials (World Scientific Publishing Company), p 4.

**Kokaj, J.; Shuaib, A.; Makdisi, Y.; Nair, R. and Mathew, J. (2018).** Femtosecond laser-based deposition of nanoparticles on a thin film and its characterization, Kuwait J. Sci. **45** (4): 37-45.

**Komaraiah, D.; Madhukar, P.; Vijayakumar, Y.; Reddy, M. and Sayanna. R. (2016).** Photocatalytic degradation study of methylene blue by brookite $TiO_2$ thin film under visible light irradiation. Mater. Today Proc. **3**: 3770– 3778.

**Liao, M.; Fang, L.; Xu, C.; Wu, F.; Huang, Q. et al. (2014).** Effect of seed layer on the growth of rutile $TiO_2$ nanorod arrays and their performance in dye-sensitized solar cells. Materials Science in Semiconductor Processing, **24**: 1-8.

**Li, X.; Han, X.; Zhu, D.; Chen, Y.; Li, L. et al. (2019).** Improvement of photoelectric properties of $TiO_2/Bi_2S_3$ composite film by annealing treatment. Optical Materials. **91**: 101-107.

**Malevu, T.; Mwankemwa, B.; Motloung, S.; Tshabalala, K. and Ocaya, R. (2019).** Effect of annealing temperature on nano-crystalline $TiO_2$ for solar cell applications. Physica E: Low-dimensional Systems and Nanostructures **106**: 127-132.

**Manikandan, K.; Ahmed, A.; Thirugnanasundar, A. and Brahmanandhan, G. (2015).** A Novel Approach to Synthesis and Characterization of Titanium Dioxide Nanoparticles for Photocatalytic Applications. Digest Journal of Nanomaterials and Biostructures, **10**(4): 1427-1437.

**Martínez, S.; Arellano, C.; González, A.; Tránsito, I.; Pérez, A. et al. (2018).** Modified sol-gel/hydrothermal method for the synthesis of microsized $TiO_2$ and iron-doped $TiO_2$, its characterization and solar photocatalytic activity for an azo dye degradation J. Photochem. Photobiol. A Chem. **359**: 93-101.

**Muaz, A.; Hashim, U.; Arshad, M.; Ruslinda, A.; Ayub, R. et al. (2015).** International Conference on Nano-electronic Technology Devices and Materials. AIP Conf. Proc. 1733: 020087.

**Oja, I.; Mere, A.; Krunks, M.; Solterbeck C. and M Souni. (2004).** Properties of $TiO_2$ Films Prepared by the Spray Pyrolysis Method.Solid State Phenomena 99-100: 259-264 (2004).

**Palmisano, L.; Augugliaro, V.; Sclafani, A. and M Schiavello. (1988).** Activity of chromium-ion-doped titania for the dinitrogen photoreduction to ammonia and for the phenol photodegradation. J. Phys. Chem., **92**: 6710-6713.

**Reddy, A.; Mallika, A.; Babu, K. and Reddy, K. (2015).** Hydrothermal Synthesis and Characterization of Zno Nano CrystalsInternational Journal of Mining Metallurgy & Mechanical Engineering, **3**(2): 2320–4060.

**Rožić, L.; Petrović, S.; Lončarević, D.; Grbić, B.; Radić, N. et al. (2019).** Influence of annealing temperature on structural, optical, and photocatalytic properties of $TiO_2$-$CeO_2$ nanopowders. Ceramics International. **45**: 2361-2367.

**Seifried, S.; Winterer, M. and H Hahn (2000).** Nanocrystalline Titania Films and Particles by Chemical Vapor Synthesis. Chem. Vap. Depos. **6**(5): 239-244.

**Soliman, M.; Al Haron, H.; Samir, M.; S Tolba, S.; Shaheen, B. et al. (2018).** On the relationship between Rutile/Anatase ratio and the nature of defect states in sub-100 nm $TiO_2$ nanostructures: experimental insights. Physical Chemistry Chemical Physics **20** (8): 5975-5982.

**Sumaryada, T.; Sofyan, A., and Syafutra, H. (2019).** Simulation of the extra-terrestrial and terrestrial performance of GaAs/Ge dual-junction solar cells Kuwait J. Sci. **46** (4): 58-65.

**Suslick K, Kirk-Othmer (1998)** encyclopedia of chemical technology 4th ed. (J. Wiley & Sons New York), p **517.**

**Tang, H.; Levy, F.; Berger, H. and Schmid, P. (1995).** Urbach tail of anatase $TiO_2$. Phys. Rev. B 52: 7771-7774.

**Tsevis, A.; Spanos, N.; Koutsoukos, P.; A. Linde, A. J. and Lyklema, J. (1998).** Preparation and characterization of anatase powders. J. Chem. Soc. Faraday Trans. **94** (2): 295-300.

**Wirunmongkol, T.; O-charoen, N. and Pavasupree, S. (2013).** Simple Hydrothermal Preparation of Zinc Oxide Powders Using Thai Autoclave Unit. Energy Procedia **34**: 801-807.

**Zgaira, I.; Alkhayatta, A.; Muhmood, A. and Hussain, S. (2019).** Investigation of structure, optical, and photoluminescence characteristics of Li doped CuO nanostructure thin films synthesized by SILAR method. Optik, **191**: 48-54.

**Zheng, S.K. (2016)** First-principles calculations of Ca/F co-doped anatase $TiO_2$. Kuwait J. Sci., **43** (2): 162-171.

**Submitted** : 18/08/2020
**Revised** : 18/10/2020
**Accepted** : 02/11/2020
**DOI** :